Kinetics of the O + HCNO Reaction

Wenhui Feng and John F. Hershberger*

Department of Chemistry and Molecular Biology, North Dakota State University, Fargo, North Dakota 58105

Received: July 18, 2007; In Final Form: August 17, 2007

The kinetics of the O + HCNO reaction were investigated by a relative rate technique using infrared diode laser absorption spectroscopy. Laser photolysis (355 nm) of NO_2 was used to produce O atoms, followed by O atom reactions with CS_2, NO_2, and HCNO, and infrared detection of OCS product from the O + CS_2 reaction. Analysis of the experiment data yields a rate constant of $k_1 = (9.84 \pm 3.52) \times 10^{-12} \exp[(-195 \pm 120)/T)]$ (cm^3 $molecule^{-1}$ s^{-1}) over the temperature range 298−375 K, with a value of $k_1 = (5.32 \pm 0.40) \times 10^{-12}$ cm^3 $molecule^{-1}$ s^{-1} at 298 K. Infrared detection of product species indicates that CO producing channels, probably CO + NO + H, dominate the reaction.

1. Introduction

Fulminic acid, HCNO, is an important intermediate in NO-reburning process for reduction of NO_x pollutants from fossil-fuel combustion emission.[1] HCNO is formed in combustion primarily by the CH_2 + NO[2−5] and HCCO + NO[6−10] reactions.

The chemistry of HCNO is therefore of great interest in the overall NO-reburning mechanism. In our laboratory, we have recently reported studies of the kinetics of the OH + HCNO, CN + HCNO, and NCO + HCNO reactions.[11−13] The experimental results show that they are all fast reactions with CO + H_2NO, NO + HCCN, and CO + NO +HCN as primary product channels, respectively. In this paper we present a kinetic study of the reaction of HCNO with $O(^3P)$ atoms. The reaction has numerous thermodynamically possible product channels:

$$O + HCNO \rightarrow HCN + O_2 \qquad \Delta H^0_{298} = -285.3 \text{ kJ/mol} \quad (1a)$$

$$\rightarrow (NCO) + OH \qquad \Delta H^0_{298} = -249.6 \text{ kJ/mol} \quad (1b)$$

$$\rightarrow HCO + NO \qquad \Delta H^0_{298} = -286.6 \text{ kJ/mol} \quad (1c)$$

$$\rightarrow CO + HNO \qquad \Delta H^0_{298} = -431.4 \text{ kJ/mol} \quad (1d)$$

$$\rightarrow CO_2 + NH \qquad \Delta H^0_{298} = -437.4 \text{ kJ/mol} \quad (1e)$$

$$\rightarrow CO + NO + H \qquad \Delta H^0_{298} = -222.7 \text{ kJ/mol} \quad (1f)$$

Thermochemical information at 298 K has been obtained from standard tables[14] as well as other references for the heats of formation of HCNO and NCO.[15]

2. Experimental Section

Infrared diode laser absorption spectroscopy was used to measure the rate constant of the title reaction by a relative rate technique. $O(^3P)$ atoms were produced by 355 nm laser photolysis of NO_2:

$$NO_2 + h\nu \text{ (355 nm)} \rightarrow NO + O(^3P) \quad (2)$$

In the presence of NO_2, HCNO, CS_2, and SF_6 buffer gas, the following reactions consume $O(^3P)$:

$$O + HCNO \rightarrow \text{products} \quad (1)$$

$$O + CS_2 \rightarrow CS + SO \quad (3a)$$

$$\rightarrow OCS + S \quad (3b)$$

$$O + NO_2 \rightarrow NO + O_2 \quad (4)$$

Among the various products in the above reactions, we chose to measure the yield of OCS (from reaction 3b) as a function of HCNO concentration.

The yields of OCS as well as several products of the title reaction were measured by infrared laser absorption spectroscopy using lead salt diode lasers (Laser Components), as described in previous publications.[11,12,16,17] IR and UV light were made collinear (6 mm beam diameter) and passed through a single-pass 143 cm absorption cell, the infrared light was detected by a 1 mm diameter InSb detector (Cincinnati Electronics, ~1 μs response time), and the resulting signal was recorded on a digital oscilloscope. Typically, only 1−2 laser shots per signal were used to eliminate errors due to depletion of the photolysis precursor or buildup of reaction products.

The HITRAN molecular database[18] was used to locate and identify the spectral lines of CO, N_2O, and CO_2 product molecules. Other published spectral data were used to locate and identify OCS,[19] HNO,[20] and HCNO[21] lines. The used absorption lines of these products were noted in Table 1. The absorption lines chosen are generally near the peak of the rotational Boltzmann distribution, minimizing sensitivity to small heating effects. Off-resonant signals were found to be negligible in these experiments.

HCNO samples were synthesized as previously described[22−24] by vacuum pyrolysis of 3-phenyl-4-oximino-isoxazol-5(4*H*)-one. The purity of the HCNO samples was characterized by FT-IR spectroscopy and was typically 95% pure or better, with only small HNCO and CO_2 impurities detected. Because HCNO

* Corresponding author. E-mail: john.hershberger@ndsu.edu.

10.1021/jp075636s CCC: $37.00
Published on Web 10/03/2007

TABLE 1: Absorption Lines Used to Probe Various Product Molecules

molecule	absorption line	line strength
OCS (00^01) ← (00^00)	R (24) at 2071.551 cm^{-1}	1.08×10^{-18}
CO ($v = 1 \leftarrow v = 0$)	P (10) at 2103.27 cm^{-1}	3.38×10^{-19}
CO_2 (00^01) ← (00^00)	P (32) at 2321.134 cm^{-1}	1.50×10^{-18}
N_2O (0001) ← (0000)	P (23) at 2202.744 cm^{-1}	7.54×10^{-19}
HNO (100) ← (000)	P (6) at 2667.785 cm^{-1}	

has poor long-term stability, samples were kept at 77 K except when filling the reaction cell. In an earlier study,[11] the thermal decomposition of HCNO in our cell was studied in detail. In general, HCNO could be allowed to stand at room temperature for ~5 min (enough for gas mixing and data collection) in our Pyrex absorption cell with minimal (~5%) decomposition. This was verified to be the case even with NO_2 and CS_2 present, indicating that no fast dark reactions were taking place. At the highest temperature used (375 K), the decomposition rate increased to about 10% over ~5 min. Experiments were limited to this narrow temperature range because the decomposition rate becomes unacceptable at higher temperatures.

CS_2 (AlfaAesar), SF_6, and CF_4 (Matheson) and were purified by repeated freeze−pump−thaw cycles at 77 K. SF_6 and CF_4 were further purified by passing through a glass column filled with Ascarite II. NO_2 (Matheson) was purified by repeated freeze−pump−thaw cycles at 200 K.

Typical experimental conditions were $P(NO_2) = 0.05$ Torr, $P(CS_2) = 0.20$ Torr, P(HCNO) = 0.5 Torr, $P(SF_6)$ or $P(CF_4) = 3.00$ Torr, and Nd: Yag laser pulse energies of 3 mJ (fluence of ~11 mJ/cm^2). CF_4 buffer gas was used for CO detection, and SF_6 buffer gas was used for detection of all other product molecules. The choice of buffer gas was motivated by the desire to relax any nascent vibrationally excited product molecules to a Boltzmann distribution.[16,17]

3. Results

3.1. Rate Constant. Figure 1 shows transient infrared absorption signals for OCS product molecules detected upon 355 nm laser photolysis of NO_2 (0.05 Torr)/CS_2 (0.20 Torr)/HCNO (variable pressures)/SF_6 (3.0 Torr) mixtures. The signals displayed a relatively fast (~70 μs) rise, followed by a slow decay. The rise is attributed to formation of OCS molecules by reaction 3b, whereas the decay is due to diffusion of OCS out of the probed volume. We note that the rise time of product molecule transient signals in these experiments is typically longer than expected on the basis of reaction kinetics alone. This is due to the likely formation of a vibrationally hot nascent distribution of molecules, which then take time (typically ~50−100 μs) to relax to the probed vibrational ground state. Our choice of buffer gas is designed to promote this vibrational relaxation.

As shown, the peak−peak amplitude of the observed OCS signals decreas with increased [HCNO], an effect attributed to the competition between reactions 1, 3, and 4 for oxygen atoms. The transient signals were converted to absolute [OCS] concentrations using tabulated HITRAN line strengths[18] as described previously,[17] by fitting the slow diffusional decay part of the signal to a linear or exponential function and extrapolating to $t = 0$. This extrapolation resulted in a typically ~3−10% correction relative to the peak−peak amplitudes. The OCS concentration data were then analyzed using reactions 1−4, as follows:

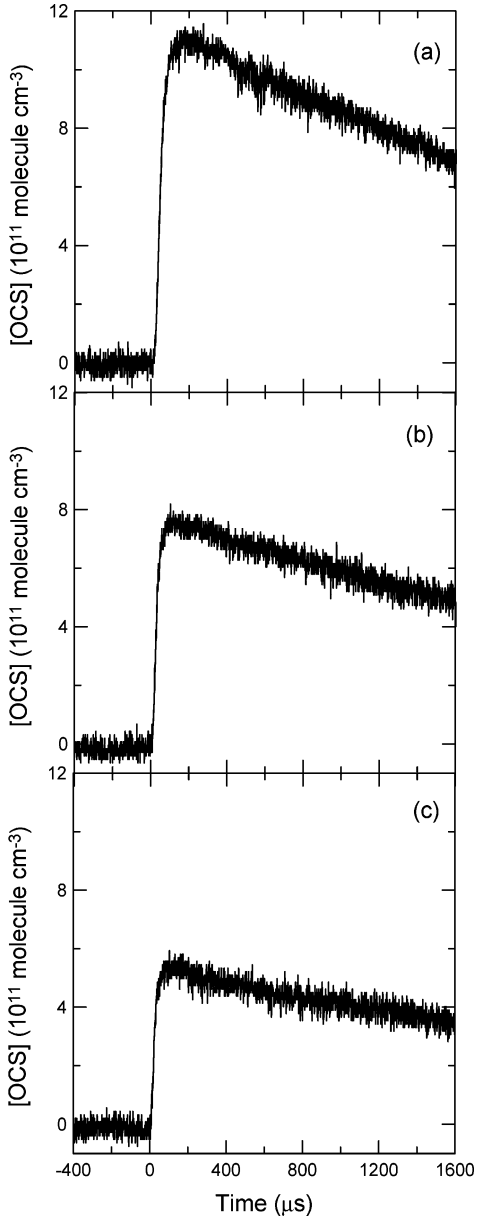

Figure 1. 1. Transient infrared absorption signal of OCS. Reaction conditions: $P(NO_2) = 0.05$ Torr, $P(CS_2) = 0.20$ Torr, $P(SF_6) = 3.0$ Torr, P(HCNO) = 0.0 Torr (trace a), 0.15 Torr (trace b), and 0.31 Torr (trace c). $T = 298$ K.

OCS was produced with a rate of

$$\frac{d[OCS]}{dt} = k_{3b}[O][CS_2] \quad (5)$$

where [O] is given by

$$[O] = [O]_0 \exp\{(-k_1[HCNO] - k_3[CS_2] - k_4[NO_2])t\} \quad (6)$$

which is obtained by the integration of

$$\frac{d[O]}{dt} = -k_1[HCNO] - k_3[CS_2] - k_4[NO_2] \quad (7)$$

As a result

$$\frac{d[OCS]}{dt} = k_{3b}[O]_0[CS_2] \exp[(-k_1[HCNO] - k_3[CS_2] - k_4[NO_2])t] \quad (8)$$

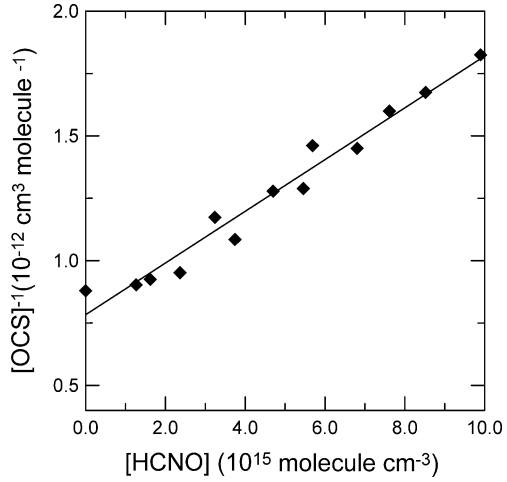

Figure 2. 2. $[OCS]^{-1}$ as a function of [HCNO]. Reaction conditions: $P(NO_2) = 0.05$ Torr, $P(CS_2) = 0.20$ Torr, $P(SF_6) = 3.0$ Torr, P(HCNO) = variable. Nd:YAG laser energy = 3.5 mJ, $T = 298$ K.

Integration of eq 8 gives

$$[OCS]_t = \frac{k_{3b}[O]_0[CS_2]}{k_1[HCNO] + k_3[CS_2] + k_4[NO_2]} \{1 - \exp[(-k_1[HCNO] - k_3[CS_2] - k_4[NO_2])t]\} \quad (9)$$

At $t = \infty$,

$$[OCS]_\infty = \frac{k_{3b}[O]_0[CS_2]}{k_1[HCNO] + k_3[CS_2] + k_4[NO_2]} \quad (10)$$

Equation 10 can be transformed to

$$\frac{1}{[OCS]_\infty} = \frac{k_1[HCNO] + k_3[CS_2] + k_4[NO_2]}{k_{3b}[O]_0[CS_2]} \quad (11)$$

Equation 11 shows that $[OCS]_\infty^{-1}$ is a linear function of [HCNO] with a slope of

$$\text{slope} = \frac{k_1}{k_{3b}[O]_0[CS_2]} \quad (12)$$

and an intercept of

$$\text{intercept} = \frac{k_3[CS_2] + k_4[NO_2]}{k_{3b}[O]_0[CS_2]} \quad (13)$$

Consequently, we can obtain k_1 from eqs 12 and 13:

$$k_1 = \left(\frac{\text{slope}}{\text{intercept}}\right) \times (k_3[CS_2] + k_4[NO_2]) \quad (14)$$

The slope and intercept can be obtained from the plot of $[OCS]_\infty^{-1}$ as the function of HCNO. Two different kinetic data compilations are in close agreement on the values of k_3 and k_4.[25,26] We use $k_3 = 3.3 \times 10^{-11} \exp[(-650 \pm 100)/T]$ (cm^3 $molecule^{-1}$ s^{-1}) and $k_4 = 5.5 \times 10^{-12} \exp[(188 \pm 81)/T]$ (cm^3 $molecule^{-1}$ s^{-1}).[25]

Figure 2 shows a plot of our experimentally obtained $[OCS]_\infty^{-1}$ as a function of [HCNO], which is predicted by eq 11 to be linear. By substituting the slope and intercept of this plot into eq 14, we determine $k_1 = (5.32 \pm 0.40) \times 10^{-12}$ cm^3 $molecule^{-1}$ s^{-1} at 298 K. Following the same procedure, we measured k_1 value at different CS_2 pressures, as shown in Table 2. The consistency in the k_1 determinations suggest that our kinetic model is valid, and no important secondary chemistry has been omitted.

TABLE 2: Rate Constants of the O + HCNO Reaction at 298 K

$[CS_2]$ (Torr)[a]	slope ($molecule^{-2}$ cm^6)	intercept (cm^3 $molecule^{-1}$)	k_1 (cm^3 $molecule^{-1}$ s^{-1})
0.05	4.23×10^{-28}	1.71×10^{-12}	$(5.50 \pm 0.56) \times 10^{-12}$
0.10	1.80×10^{-28}	1.05×10^{-12}	$(4.84 \pm 0.32) \times 10^{-12}$
0.20	1.04×10^{-28}	7.83×10^{-13}	$(5.32 \pm 0.37) \times 10^{-12}$

[a] Other reaction conditions: $P(NO_2) = 0.05$ Torr, $P(SF_6) = 3.0$ Torr, and P(HCNO) = variable, YAG laser power = 3.5 mJ.

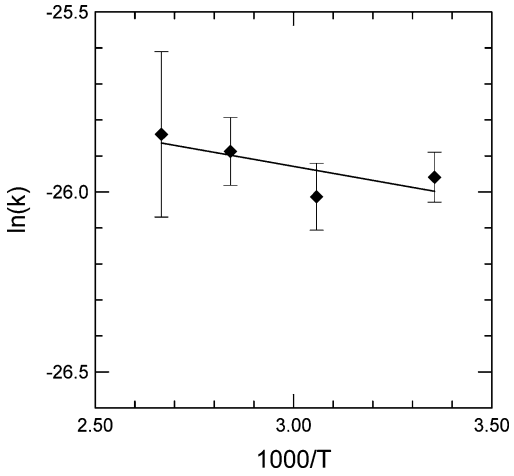

Figure 3. 3. Arrhenius plot for the O + HCNO reaction over the temperature range 298−375 K.

Similar experiments were performed at elevated temperatures. Figure 3 shows an Arrhenius plot of the resulting kinetic data for the O + HCNO reaction. Measurements were limited to a rather narrow temperature range of 298−375 K, because HCNO decomposition in the reaction cell becomes unacceptably rapid at higher temperatures.[11] Nevertheless, the temperature range is sufficient to obtain reasonably precise Arrhenius parameters. We obtain the following rate constants (error bars represent one standard deviation):

$$k_1(T) = (9.84 \pm 3.52) \times 10^{-12} \times \exp[(-195 \pm 120)/T] \text{ (cm^3 $molecule^{-1}$ s^{-1})}$$

3.2. Product Yields. Infrared diode laser absorption was used to attempt detection of products upon 355 nm photolysis of NO_2 (0.05 Torr)/HCNO (0.45 Torr)/buffer gas (1.5 Torr) mixtures. (Noted as R1 mixtures in the following section.) All detection experiments were conducted at 298 K. Previous experiments on HCNO kinetics in our laboratory[11−13] used 248 nm photolysis, which resulted in substantial background signals due to 248 nm absorption and resulting photolysis of HCNO. The absorption coefficient of HCNO at 355 nm is much smaller, however, resulting in only traces of products observed in the absence of the NO_2 precursor.

Figure 4 shows typical transient infrared absorption signals of products. As shown, a large CO signal and a significant CO_2 signal were detected upon 355 nm photolysis of R1 mixtures. Detection of HNO products was attempted, but no signal was observed. Nitric oxide (NO) is expected to be produced in channel 1f, but we did not attempt to detect this species, due to the large interferences of NO products from both reactions 2 and 4.

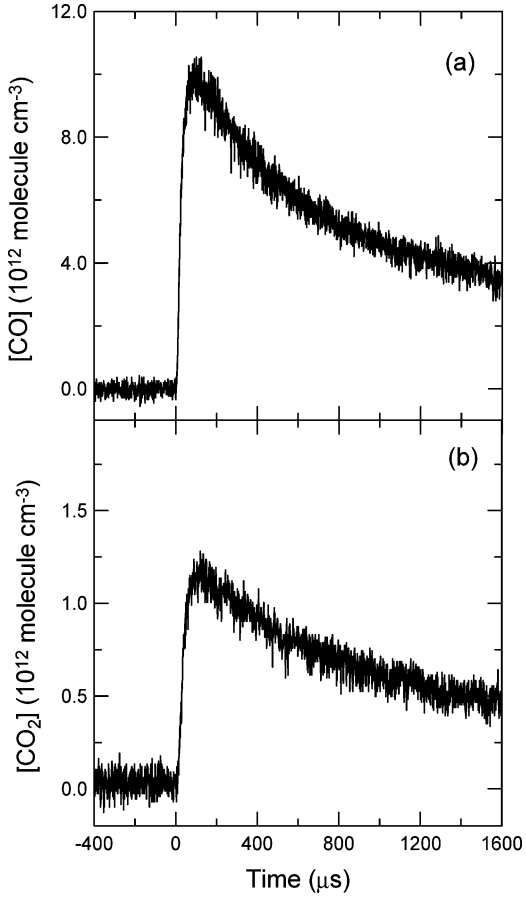

Figure 4. 4. Transient infrared absorption signals of (a) CO and (b) CO_2. Reaction conditions: $P(NO_2) = 0.05$ Torr, $P(HCNO) = 0.5$ Torr, $P(CF_4) = 1.5$ Torr (for CO transient only), $P(SF_6) = 1.5$ Torr (CO_2 transient only), Nd:YAG laser energy = 3.0 mJ, $T = 298$ K.

To investigate the importance of channels 1b, 1c, and 1e, we attempted to detect N_2O and HNO upon photolysis of NO_2 (0.05 Torr)/HCNO (0.45 Torr)/NO (0.5 Torr)/SF_6 (1.5 Torr) mixtures (noted as R2 mixtures in the following section). By including an excess of NO in these reaction mixtures, we ensure that many of the radicals potentially formed in reaction 1 react with NO. Such reactions are generally quite well characterized in the literature.[17,27] For example, as CO_2 was detected, one might expect NH radicals to be also formed via reaction 1e. If an excess of NO is included in the reaction mixture, the following reaction is expected:

$$NH + NO \rightarrow N_2O + H \quad (15a)$$

$$\rightarrow N_2 + OH \quad (15b)$$

(Product branching ratio at 298 K: $\varphi_{15a} = 0.77$.[27]) Furthermore, N_2O may also be created by a secondary reaction of NCO radicals created in channel 1b:

$$NCO + NO \rightarrow N_2O + CO \quad (16a)$$

$$\rightarrow N_2 + CO_2 \quad (16b)$$

(Product branching ratios at 296 K: $\varphi_{16a} = 0.44$; $\varphi_{16b} = 0.56$.[17]) Similarly, if channel 1c is significant, HNO should be detected from the secondary reaction of HCO with NO:

$$HCO + NO \rightarrow HNO + CO \quad (17)$$

TABLE 3: Product Yields of the Reaction O + HCNO[a]

product	yield (10^{12} molecule cm^{-3})	relative yield[b]
CO	11.8 ± 1.0	1
CO_2	1.33 ± 0.2	0.11
HNO	≤ 0.98	≤ 0.08
HNO[c]	≤ 1.4	≤ 0.12
N_2O[c]	≤ 0.07	≤ 0.006

[a] Reaction condition: $P(NO_2) = 0.05$ Torr, $P(HCNO) = 0.45$ Torr, $P(SF_6) = 1.5$ Torr, YAG laser power = 3.0 mJ. [b] Obtained by normalizing to [CO] = 1.00. [c] Detected in the presence of 0.5 Torr NO (i.e., R2 mixture).

In these experiments, no signals attributable to N_2O or HNO were detected upon 355 nm photolysis of R2 mixtures, suggesting that reaction channels 1b, 1c, and 1e are at most minor contributions to the title reaction.

HCN from channel 1a is not detectable in our diode laser spectroscopy because of the lack of available laser diodes in the HCN spectral region. As a result, we cannot probe the importance of channel 1a by transient infrared spectroscopy. We have, however, obtained static FT-IR spectra of R1 mixtures before and after extensive photolysis (~1000 355-nm Nd:YAG laser pulses). The stable products observed in the transient experiments are observable in the FT-IR, but no HCN was detected.

Transient signal amplitudes (peak−peak) were converted into absolute concentration using HITRAN line-strengths, except for HNO molecules, for which we used absorption coefficients previously measured in our laboratory.[11] For those product molecules that we failed to detect, we give an upper limit on basis of the noise level. Table 3 shows a typical dataset of product molecule yields. The right-hand column of Table 3 shows the resulting relative product yield.

Clearly, CO molecules are the dominant product. Several sources of CO are possible in this system. Obviously, channels 1d and 1f can be a direct resource of CO molecules. Channel 1c can lead to CO molecules by the secondary reaction of HCO with NO_2 or HCO decomposition to H + CO:

$$HCO + NO_2 \rightarrow CO + NO + OH \quad (18a)$$

$$\rightarrow NO + H + CO_2 \quad (18b)$$

$$HCO \rightarrow CO + H \quad (19)$$

(Product branching ratio at 296 K: $\varphi_{18a} = 0.63$.[28]) Channel 1b can finally lead to CO molecules via the secondary reactions of both NCO and OH with HCNO:

$$NCO + HCNO \rightarrow CO + NO + HCN \quad (20)$$

$$OH + HCNO \rightarrow CO + H_2NO \quad (21a)$$

$$\rightarrow HCO + HNO \quad (21b)$$

(Product branching ratio at 296 K: $\varphi_{20} = 0.92$, $\varphi_{21a} = 0.61$, $\varphi_{21b} = 0.35$.[11,13]) The HCO product in (21b) can continue to produce CO molecules via reactions 18 and 19. The lack of HNO or N_2O detection upon photolysis of R2 mixtures, however, results in upper limits for the contributions of channels 1b, 1c, and 1d. On the basis of our upper limits, we estimate that these channels can contribute at most to ~20% of our observed CO yield. (The contribution is probably less than this, but we are being conservative because of uncertainties such as the fact that not every NH, NCO, or HCO radical may react with NO in our R2 mixtures; some may react with other reagents in the gas mixture. Uncertainties regarding reactions such as

TABLE 4: Product Branching of the Reaction O + HCNO[a]

channel[b]	yield of italicized product[c]	branching ratio (%)[d]
CO + NO + H (1f)	≥0.40	≥74
CO_2 + *NH* (1e)	≤0.01	≤2
CO + *HNO* (1d) and *HCO* + NO (1c)	≤0.12	≤22
NCO + OH (1b)	≤0.01	≤2

[a] Assumes other potential channels are not active. [b] The yields of italic molecules are used to determine the branching ratios. [c] Based on relative yields of Table 3. [d] Obtained by normalizing the total relative yield of all listed channels to 1.

NH + HCNO, HCO + HCNO, etc. make detailed modeling difficult.) We estimate that the rest (~80%) of the observed CO molecules originate from channel 1f and resulting secondary chemistry of H atoms:

$$H + NO_2 \rightarrow OH + NO \quad (22)$$

followed by reaction 21. The effect of reaction 22 followed by reaction 21 is that each H atom produced in channel 1f would result in another CO molecule, therefore roughly doubling the CO yield.

We, therefore, as a crude estimate, obtain a branching ratio for channel 1f as follows. First, we suggest that it is likely that most of the observed CO_2 yield is not from channel 1e, which would also produce NH and therefore N_2O in R2 mixtures, but is from secondary chemistry such as reaction 18b, where the HCO originated either from channel 1c or reaction 21b. We use the upper limit on N_2O formation to conclude that (1b) and (1e) are insignificant channels. We then estimate the total relative CO yield as

$$[CO]_{1f} \times 2 + [CO]_{other} = 1.00 \quad (23)$$

where 1.00 is our total relative CO yield, $[CO]_{other}$ is the relative CO yield from channels 1b, 1c, and 1d and associated secondary chemistry, and $[CO]_{1f}$ is the relative CO yield from channel 1f. The factor of 2 represents the approximate doubling of the CO produced in (1f) by reactions 22 and 21. Using an upper limit of $[CO]_{other} = 0.20$, we obtain a lower limit of $[CO]_{1f} \geq 0.40$. Using upper limits of [HNO] + [HCO] ≤ 0.12, we then normalize the sum of $[CO]_{1f}$, [HNO], [HCO], [NCO], and [NH] to unity to obtain approximate branching ratios shown in Table 4. In summary, we suggest that channel 1f contributes at least ~74% to the title reaction. Our very low upper limit on N_2O formation rules out channels 1b and 1e as significant contributors, but our rather high upper limit on HNO formation implies that channels 1c and/or 1d may have minor, but significant, contributions.

4. Discussion

In their theoretical study of HCNO kinetics, Miller et al. suggested a fast rate constant of 1.16×10^{-10} cm^3 molecule^{-1} s^{-1} without temperature dependence for the title reaction.[1,29] Our results represent the first experimental study of the reaction, showing this is actually a rather slow reaction at room temperature. In contrast to other reactions of radicals with HCNO,[11−13] which display significant negative activation energies, the O + HCNO reaction displays virtually no temperature dependence over the measured range, with a very small positive activation energy of ~0.4 kcal/mol.

Possible complications from secondary chemistry may include reactions of CS and SO molecules produced in reaction 3:

$$CS + HCNO \rightarrow OCS + HCN \quad (24)$$

$$SO + HCNO \rightarrow OCS + HNO \quad (25)$$

No kinetic studies of these reactions have been reported, but we note that in general CS is a quite unreactive species. For example, reactions of CS with NO_2, O_2, and O_3 are all very slow.[30] We believe reaction 23 must be also very slow, partly because it would tend to result in an increased OCS yield at higher HCNO concentrations, which is contrary to our experimental data. SO radicals are probably consumed by NO_2:

$$SO + NO_2 \rightarrow NO + SO_2 \quad (26)$$

with a rate constant of $k_{26} = 1.4 \times 10^{-11}$ cm^3 molecule^{-1} s^{-1},[25] and therefore do not affect our results.

Another possible issue in these experiments is the possibility that the results are affected by concentration gradients down the length of the reaction cell. Using a literature value[31] for the 355 nm absorption cross section of NO_2, $\sigma_{355} = 5 \times 10^{-19}$ cm^2, $P(NO_2) = 0.05$ Torr, and $l = 143$ cm, we estimate that ~11% of the photolysis light is absorbed over the cell path length, resulting in a modest $[O]_0$ gradient. We note, however, that the data analysis does not require precise knowledge of $[O]_0$, as it affects both the slope and intercept (eqs 12 and 13) equally, and it is the ratio of slope to intercept that is used in eq 14 to determine the rate constant. An $[NO_2]$ concentration gradient would present a more serious problem, because $[NO_2]$ appears in eq 14, but at our photolysis pulse energies, we estimate that only ~1% of the NO_2 is dissociated per pulse.

5. Conclusion

The kinetics of the O + HCNO reaction was studied using diode laser infrared absorption spectroscopy. The rate constant of the reaction can be expressed by $k_1(T) = (9.84 \pm 3.52) \times 10^{-12} \exp[(-195 \pm 120)/T]$ (cm^3 molecule^{-1} s^{-1}) over the temperature range 298−375 K. Products detected include CO and a minor amount of CO_2, suggesting that CO producing channels, probably CO + NO + H, dominate the reaction.

Acknowledgment. This work was supported by Division of Chemical Sciences, Office of Basic Energy Sciences of the U.S. Department of Energy, Grant DE-FG03-96ER14645. Partial support from ND EPSCoR through NSF grant no. EPS-0447679 is also acknowledged.

References and Notes

(1) Miller, J. A.; Klippenstein, S. J.; Glarborg, P. *Combust. Flame* **2003**, *135*, 357.
(2) Zhang, W. C.; Du, B. N.; Feng, C. J. *J. Mol. Struct. (THEOCHEM)* **2004**, *679*, 121.
(3) Eshchenko, G.; Kocher, T.; Kerst, C.; Temps, F. *Chem. Phys. Lett.* **2002**, *356*, 181.
(4) Bauerle, S.; Klatt, M.; Wagner, Gg. H. *Ber. Bunsen-Ges. Phys. Chem.* **1995**, *99*, 97.
(5) Grussdorf, J.; Temps, F.; Wagner, Gg, H. *Ber. Gunsen-Ges. Phys. Chem.* **1997**, *101*, 134.
(6) Meyer, J. P.; Hershberger, J. F. *J. Phys. Chem. B* **2005**, *109*, 8363.
(7) Vereecken, L.; Sumathy, R.; Carl, S. A.; Peeters, *J. Chem. Phys. Lett.* **2001**, *344*, 400.
(8) Tokmakov, I. V.; Moskaleva, L. V.; Paschenko, D. V.; Lin, M. C. *J. Phys. Chem. A* **2003**, *107*, 1066.
(9) Rim, K. T.; Hershberger, J. F. *J. Phys. Chem. A* **2000**, *104*, 293.
(10) Eickhoff, U.; Temps, F. *Phys. Chem. Chem. Phys.* **1999**, *1*, 243.
(11) Feng, W.; Meyer, J. P.; Hershberger, J. F. *J. Phys. Chem. A* **2006**, *110*, 4458.
(12) Feng, W.; Hershberger, J. F. *J. Phys. Chem. A* **2006**, *110*, 12184.
(13) Feng, W.; Hershberger, J. F. *J. Phys. Chem. A.* **2007**, *111*, 3831.
(14) Chase, M. W. NIST-JANAF Thermochemical Tables, 4th ed. *J. Phys. Chem. Ref. Data*, **1998**.

(15) Schuurman, M. S.; Muir, S. R.; Allen, W. D.; Schaefer H. F., III,. *J. Chem. Phys*. **2004**, *120*, 11586.
(16) Cooper, W. F.; Hershberger, J. F. *J. Phys. Chem.* **1992**, *96*, 771.
(17) Cooper, W. F.; Hershberger, J. F. *J. Phys. Chem.* **1992**, *96*, 5405.
(18) Rothman, L. S.; et al. *J. Quantum Spectrosc. Radiat. Transfer* **1992**, *48*, 469.
(19) Hunt, N.; Foster, S. C.; Johns, J. W. C.; McKellar, A. R. W. *J. Mol. Spectrosc.* **1985**, *111*, 42.
(20) Johns, J. W. C.; McKellar, A. R. W.; Weinberger, E. *Can. J. Phys.* **1983**, *61*, 1106.
(21) Ferretti, F. L.; Rao, K. N. *J. Mol. Spectrosc.* **1974**, *51*, 97.
(22) Pasinszki, T.; Kishimoto, N.; Ohno, K. *J. Phys. Chem.* **1999**, *103*, 6746.
(23) Wentrup, C.; Gerecht, B.; Briehl, H. *Angew. Chem., Int. Ed. Engl*. **1979**, *18*, 467.
(24) Wilmes, R.; Winnewisser, M. *J. Labelled Compd. Radiopharm*. **1993**, *33*, 157.
(25) Atkinson, R.; Baulch, D. L.; Cox, R. A.; Crowley, J. N.; Hampson, R. F.; Hynes, R. G.; Jenkin, M. E.; Rossi, M. J.; Troe, J. *Atmos. Chem. Phys.* **2004**, *4*, 1461.
(26) *Chemical Kinetics and Photochemical Data for Use in Atmospheric Studies*; Evaluation Number 15; JPL publication 2006-2; JPL: Pasadena, CA, 2006.
(27) Quandt, R. W.; Hershberger, J. F. *J. Phys. Chem.* **1995**, *99*, 16939.
(28) Rim, K. T.; Hershberger, J. F. *J. Phys. Chem. A* **1998**, *102*, 5898.
(29) Miller, J. A.; Durant, M. C.; Glarborg, P. *Proc. Combust. Inst.* **1998**, *27*, 234.
(30) Black, G.; Jusinski, L. E.; Slanger, T. G. *Chem. Phys. Lett*. **1983**, *102*, 64.
(31) Okabe, H. *Photochemistry of Small Molecules*; Wiley-Interscience: New York, 1978.